Journal of Energy Chemistry 000 (2018) 1–7

Contents lists available at ScienceDirect

Journal of Energy Chemistry

journal homepage: www.elsevier.com/locate/jechem

http://www.journals.elsevier.com/journal-of-energy-chemistry/

Fast, green microwave-assisted synthesis of single crystalline Sb_2Se_3 nanowires towards promising lithium storage

Wen Luo[a,b], Jean-Jacques Gaumet[b,*], Pierre Magri[b], Sébastien Diliberto[c], Feng Li[a], Pascal Franchetti[b], Jaafar Ghanbaja[c], Liqiang Mai[a,*]

[a] State Key Laboratory of Advanced Technology for Materials Synthesis and Processing, Wuhan University of Technology, Wuhan 430070, Hubei, China
[b] Laboratoire de Chimie et Physique: Approche Multi-échelles des Milieux Complexes, Institut Jean Barriol, Université de Lorraine, Metz 57070, France
[c] Institut Jean Lamour, UMR CNRS 7198, Université de Lorraine, Campus Artem, 2 allée André Guinier, Nancy 54000, France

ARTICLE INFO

Article history:
Received 13 February 2018
Revised 23 March 2018
Accepted 26 March 2018
Available online xxx

Keywords:
Microwave synthesis
Sb_2Se_3 nanowires
Solvent-mediated process
Lithium-ion battery
High-performance anode

ABSTRACT

In this work, a fast (0.5 h), green microwave-assisted synthesis of single crystalline Sb_2Se_3 nanowires was developed. For the first time we demonstrated a facile solvent-mediated process, whereby intriguing nanostructures including antimony selenide (Sb_2Se_3) nanowires and selenium (Se) microrods can be achieved by merely varying the volume ratio of ethylene glycol (EG) and H_2O free from expensive chemical and additional surfactant. The achieved uniform Sb_2Se_3 nanowire is single crystalline along [001] growth direction with a diameter of 100 nm and a length up to tens of micrometers. When evaluated as an anode of lithium-ion battery, Sb_2Se_3 nanowire can deliver a high reversible capacity of 650.2 mAh g^{-1} at 100 mA g^{-1} and a capacity retention of 63.8% after long-term 1000 cycles at 1000 mA g^{-1}, as well as superior rate capability (389.5 mAh g^{-1} at 2000 mA g^{-1}). This easy solvent-mediated microwave synthesis approach exhibits its great universe and importance towards the fabrication of high-performance metal chalcogenide electrode materials for future low-cost, large-scale energy storage systems.

1. Introduction

Main-group V–VI metal chalcogenides semiconductors are of great technological importance because of their typical narrow band gap and size-dependent properties [1]. Among these compounds, antimony selenide (Sb_2Se_3) is one kind of representative direct band-gap semiconductors ($E_g \approx 1.11$ eV) and has held promise in the applications of optoelectronic [2], thermoelectrics [3], photovoltaics [4,5] and electrochemical energy storage [6–9]. Various novel Sb_2Se_3 nanostructures exhibit different physical and chemical properties compared with their bulk counterparts. Notably one-dimensional (1D) Sb_2Se_3 nanostructures demonstrate unique properties due to their anisotropic shape, especially 1D nanowires with high aspect ratio [2,10]. Of particular note that Sb_2Se_3 has captured great attentions as an anode for lithium-ion batteries (LIBs) and sodium-ion batteries (SIBs) due to its high theoretic capacity of 670 mAh g^{-1} [7,11]. The synthesis and fabrication of high-performance Sb_2Se_3 anode for LIBs is of great interest to researchers in the field of energy and chemistry.

To date, much effort has been devoted to the fabrication of 1D Sb_2Se_3 nanostructures. Various approaches have been developed, such as hydrothermal/solvothermal synthesis [12–18], sol–gel route [19], microwave-assisted method [20,21], template-assisted approach [22], vapor liquid solid (VLS) method [23] and gas-induced reduction method [24]. However, as far as we know, most of previous studies involve high-toxic reducing agent, time-consuming protocol and exhibit low yield feature. For instance, the common exploited hydrothermal method usually requires a long-time (6–72 h) high-temperature treatment to promote the complete splitting growth of Sb_2Se_3 nanowires [2,7]. In addition, some involved surfactant or template reagents are hardly to be totally removed, which is unfavorable for the quality of Sb_2Se_3 nanowires. Although gas-induced growth of Sb_2Se_3 nanowires seems to be an effective route to achieve high-crystallinity product, the special condition and complex procedures restrict the large-scale synthesis [24]. Therefore, developing a rapid, green, high-yield synthesis of uniform Sb_2Se_3 nanowires is still highly desired.

Recently microwave-assisted synthesis exhibits superior advantages towards the fabrication of nanomaterials because the microwave irradiation can lead to fast nucleation and greatly shorten the reaction time [25]. Specifically, in the presence of suitable polyol solvents which can induce a reducing and coordinating

* Corresponding authors.
E-mail addresses: jean-jacques.gaumet@univ-lorraine.fr (J.-J. Gaumet), mlq518@whut.edu.cn (L. Mai).

https://doi.org/10.1016/j.jechem.2018.03.013

Please cite this article as: W. Luo et al., Fast, green microwave-assisted synthesis of single crystalline Sb_2Se_3 nanowires towards promising lithium storage, Journal of Energy Chemistry (2018), https://doi.org/10.1016/j.jechem.2018.03.013

environment, a certain degree of size and shape control can be facilely established compared to that in pure aqueous or monofunctional alcohol media [26–28]. For example, Zhao et al. employed microwave irradiation to obtain Sb_2Se_3 nanowires in oleylamine which acts as both the reducing solvent and the medium of microwave heating [20]. Zhou and Zhu reported the synthesis of Sb_2Se_3 submicron rods based on the polyol reducing process [29]. In our work, a fast (0.5 h) and green solvent-mediated microwave synthesis of uniform single crystalline Sb_2Se_3 nanowires was developed. In a simple ethylene glycol (EG)/H_2O solvent system free from any further surfactant or template, Sb_2Se_3 nanowires and Se microrods can be achieved by merely varying the volume ratio of EG and H_2O. Impressively, when evaluated as an anode of LIBs, Sb_2Se_3 nanowires exhibit good cycling stability and outstanding rate performance: it can deliver a high reversible capacity of 650.2 mAh g^{-1} at 100 mA g^{-1} and a capacity retention of 63.8% after long-term 1000 cycles at 1000 mA g^{-1}, as well as superior rate capability (389.5 mAh g^{-1} at 2000 mA g^{-1}). We believe that our facile approach provides a new idea for the design of metal chalcogenide, a better utilization of microwave irradiation to synthesize nanostructures in green solvents, and demonstrates its potential application in energy storage systems.

2. Experimental

2.1. Synthetic procedures

All reactants and solvents were analytical grades and used without further purification. Microwave irradiation experiments were carried out using a Monowave 300 single-mode microwave reactor from Anton Paar GmbH (Graz, Austria). Microwave synthesis was performed in 30 mL Pyrex vials that were sealed with PEEK snap caps and standard polytetrafluoroethylene (PTFE)-coated silicone septa. The typical synthesis of Sb_2Se_3 nanowires is as follows: First, 0.114 g $SbCl_3$ (0.5 mmol) and 0.13 g Na_2SeO_3 (0.75 mmol) were dissolved in the 20 mL deionized water (H_2O) under magnetic stirring for 1 h. Second, 0.1 g $NaBH_4$ was rapidly added into solution with continuous magnetic stirring. Next, the mixed solution was transferred to a 30 mL vial for microwave irradiation. During a typical run, the microwave power was adjusted to heat the sample to 180 °C as fast as possible, and then the temperature was maintained for 0.5 h with a stirring rate of 600 rpm. After the vial was naturally cooled to room temperature, black precipitate was collected by centrifugation and was washed thoroughly with anhydrous ethanol and deionized water for three times respectively. The collected precipitate was dried in vacuum at 70 °C overnight for later characterization. For the preparation of comparison samples, the solvent was replaced by the mixture of EG and H_2O with different volume ratios: namely, 0 mL EG + 20 mL H_2O (the achieved sample denoted as E0); 5 mL EG + 15 mL H_2O (E5); 10 mL EG + 10 mL H_2O (E10); 15 mL EG + 5 mL H_2O (E15); 20 mL EG + 0 mL H_2O (E20). And other conditions remained same to investigate the solvent-mediated effect.

2.2. Characterization

Field emission scanning electron microscopy (FESEM) images were collected with a TescanVega3 microscope equipped with a XFlash detector 410 M (Bruker) for energy-dispersive X-ray (EDX) analysis. X-ray diffraction (XRD) patterns were obtained with a Bruker AXS D8 Advance diffractometer using a Cu anode (λ Cu $K\alpha = 1.5406$ Å). Transmission electron microscopy (TEM) and high-resolution TEM (HRTEM) images were recorded using a JEM-ARM 200F Cold FEG TEM/STEM operating at 200 kV and equipped with a spherical aberration (Cs) probe cornt resolution 0.19 nm in TEM mode and 0.078 nm in STEM mode fitted with a GIF Quantum ER. Raman spectra were collected through a Renishaw inVia Raman microscope. A 632.8 nm He–Ne laser was focused on the samples and no filter was used. Thermogravimetric analysis (TGA) and differential scanning calorimetry (DSC) tests were respectively performed on TGA Q50 and a DSC Q2000 from TA Instruments. The thermal evolution was conducted from room temperature up to 600 °C with a continuous heating rate of 10 °C min^{-1} under flow nitrogen protection at the flow rate of 40 mL min^{-1}. pH value measurements were carried on a pH meter PHM210 from Radiometer with a combined probe.

2.3. Electrochemical measurement

The electrochemical performance was evaluated by assembly of 2016-type coin cells in a glove box filled with pure argon gas. The electrodes were prepared by a mixed slurry with a weight ratio of 70% Sb_2Se_3 nanowire active material, 20% ketjen black and 10% carboxy methyl cellulose (CMC aqueous solution). The mixed slurry was pasted on copper foil and dried in an oven at 70 °C for 12 h. The average mass loading was approximately 1.1 mg cm^{-2}. In lithium half cells, lithium metal was used as the counter electrode. 1 M $LiPF_6$ in ethylene carbon (EC)/ dimethyl carbonate (DMC)/ ethyl methyl carbonate (EMC) (1/1/1 vol/vol/vol) was used as electrolyte. A Whatman glass fibre membrane (GF/D) was used as the separator. Galvanostatic charge–discharge measurement was performed using a multi-channel battery testing system (LAND CT2001A). Cyclic voltammetry (CV) curves and electrochemical impedance spectrum (EIS) were recorded with an electrochemical workstation at different scan rates (Autolab PGSTAT 302). EIS test was performed with a frequency range of 0.01–10^5 Hz.

3. Results and discussion

To study the influence of mixture solvent on the morphology and composition, controllable experiments were performed by merely changing the volume ratio of EG/H_2O. SEM images and corresponding XRD patterns of the as-prepared five products with the increasing amount of EG from 0 to 20 mL are depicted in Fig. 1. It is found that if no EG was added in the reaction system, uniform and dispersive nanowires were formed (Fig. 1(a)). The corresponding XRD pattern of sample E0 demonstrates that all the diffraction peaks can be well indexed as an orthorhombic phase of Sb_2Se_3 without any detectable impurity (JCPDS 01-075-1462) (Fig. 1(b)). If 5 mL EG was introduced in the solvent system, even shorter and less uniform nanowires were also achieved (Fig. 1(c)). Notably, a large number of irregular nanoparticles and nonuniform nanowires coexist when the amount of EG was increased to 10 mL (Fig. 1(e)). Interestingly, except diffraction peaks indexed to Sb_2Se_3, some weak peaks ascribed to hexagonal Se (JCPDS 01-073-0456) are evident in both XRD patterns of sample E5 (Fig. 1(d)) and sample E10 (Fig. 1(f)). It should be carefully noted that one small diffraction peak located at $2\theta = 13.2°$ detected in both XRD patterns of sample E5 (Fig. 1(d)) and sample E10 (Fig. 1(f)) is associated with a kind of hydrogen antimony oxide hydrate ($HSbO_3(H_2O)_{0.267}$, JCPDS: 01-083-1928). These results indicate that the multicomponent mixture of orthorhombic phase Sb_2Se_3, crystalline Se along with antimony oxide hydrate would somehow be obtained in such reduction environment due to the presence of mixture solvents. Notably here as the volume of EG was increased to 15 mL, a dramatic change in morphology occurred: no nanowire was formed and instead micrometer-sized short bundles and rods were obtained (Fig. 1(g)). XRD pattern of sample E15 reveals that all the diffraction peaks can be indexed to hexagonal Se (JCPDS 01-073-0456) (Fig. 1(h)). These results suggest that when the amount of EG excess that of H_2O, the chemical environment of reaction system has completely changed, which induce the formation of products

Please cite this article as: W. Luo et al., Fast, green microwave-assisted synthesis of single crystalline Sb_2Se_3 nanowires towards promising lithium storage, Journal of Energy Chemistry (2018), https://doi.org/10.1016/j.jechem.2018.03.013

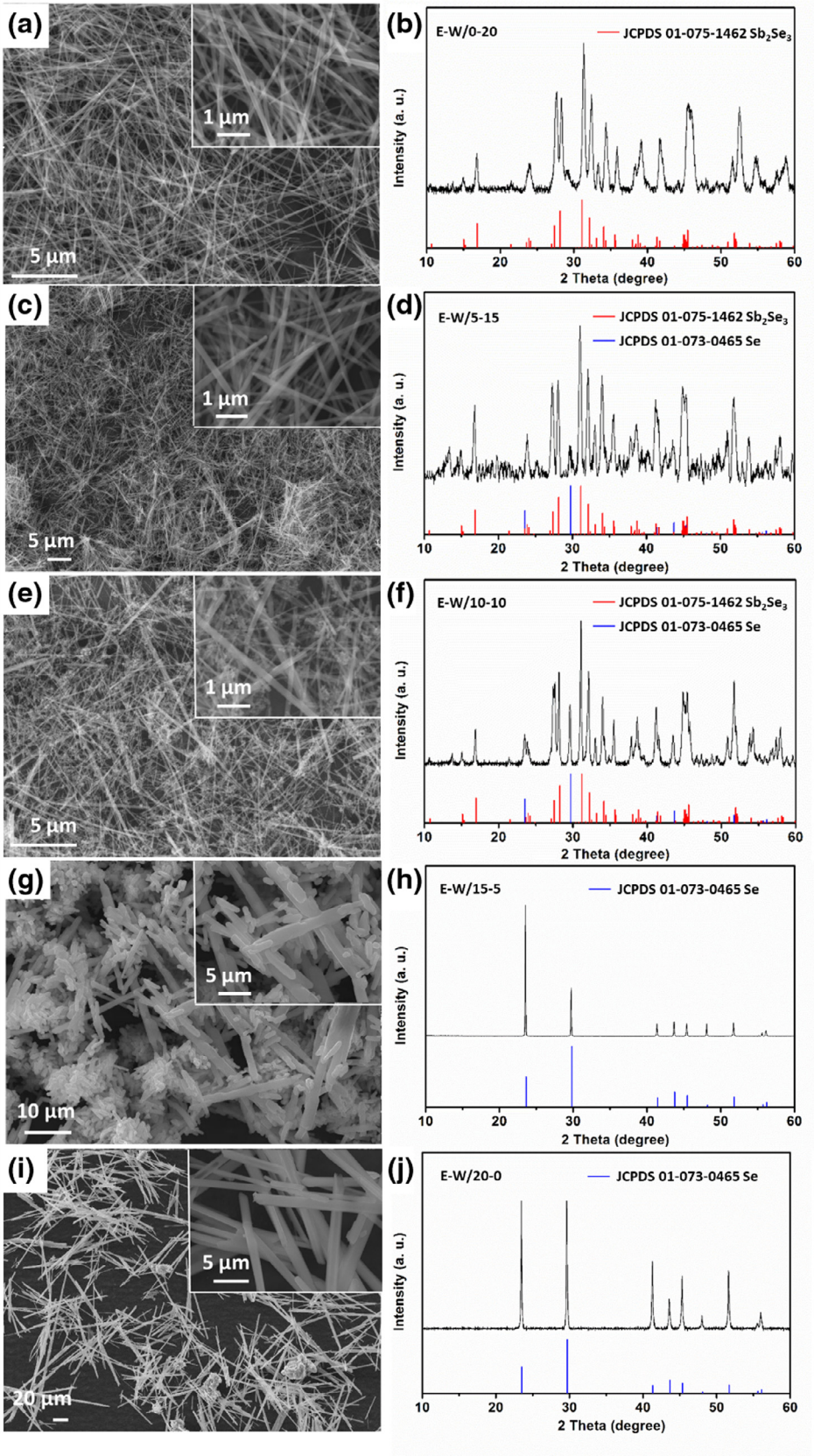

Fig. 1. SEM images of (a) sample E0, (c) sample E5, (e) sample E10, (g) sample E15, (i) sample E20 and the corresponding XRD patterns of (b) sample E0, (d) sample E5, (f) sample E10, (h) sample E15, (j) sample E20.

Please cite this article as: W. Luo et al., Fast, green microwave-assisted synthesis of single crystalline Sb_2Se_3 nanowires towards promising lithium storage, Journal of Energy Chemistry (2018), https://doi.org/10.1016/j.jechem.2018.03.013

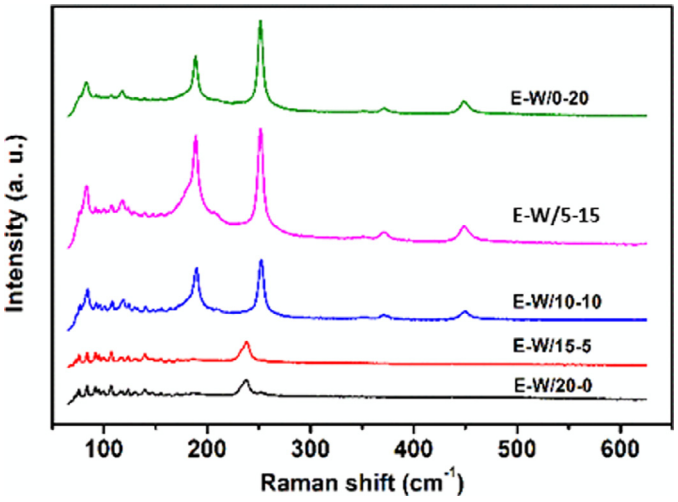

Fig. 2. Raman spectra of sample E0, E5, E10, E15 and E20.

in different phases and morphologies. The key linkages between all experimental factors will be discussed in the subsequent text. Still, when the amount of EG was further increased to 20 mL, namely in a total EG solvent reaction system, uniform 1D rods about 2 μm in diameter and tens of micrometers in length were formed (Fig. 1(i)). XRD result shows that these microrods products are pure phase hexagonal Se (JCPDS 01-073-0456) (Fig. 1(j)). The facile synthesis of 1D hexagonal phase Se microstructure also exhibits great potential in related applications, such as Li–Se batteries [30] and Se-based solar cells [31]. More importantly, our method comprises merits of green reducing agent, short reaction time and high-quality nanowires product compared to previous reports on the synthesis of Sb_2Se_3 via wet chemical approaches (See supporting information, Table S1).

DSC and TGA measurements were carried out to identify the composition of as-prepared samples. As clearly demonstrated in Fig. S1, samples E0, E5 and E10 mainly contain large portions of Sb_2Se_3. The amounts of Se colloids in the E0, E5 and E10 composites were determined to be only 0.6 wt% (Fig. S1(a)), 3 wt% (Fig. S2(b)) and 5 wt% (Fig. S1(c)), respectively. These TGA results match well with above XRD analysis, confirming that in H_2O-excess systems the increase of EG would favor the formation of more Se colloids. Meanwhile, sample E15 and sample E20 contain 76 wt% Se (Fig. S1(d)) and 96 wt% Se (Fig. S1(e)) respectively, which further confirm that the resulted products are Se rods.

Raman spectra of above five samples were provided in Fig. 2. Six intensive sharp peaks were obviously observed for three types of Sb_2Se_3 composites (E0, E5 and E10). In details, the peaks located at 83 cm^{-1} are ascribed to the translational vibration of Se−Sb−Se. The bands at 118 and 189 cm^{-1} are due to Se–Sb–Se bending. The vibrations at 252, 372 and 450 cm^{-1} originate from Sb−Se stretching. The Raman mode assignments are in accordance with previous reports [32], demonstrating the high quality of as-prepared Sb_2Se_3 composites. In contrast, no typical Raman mode assigned to Sb_2Se_3 can be detected in Se composites (E15 and E20). The only notable mode located at 238 cm^{-1} can be assigned to Se−Se stretching when materials are completely crystallized [33].

To provide further insights into the microstructure of Sb_2Se_3 nanowires, the detailed morphology and structure characterizations of sample E0 were conducted as follow. The typical SEM images of Sb_2Se_3 nanowires were shown in Fig. 3(a)–(c). The low magnification SEM image presented in Fig. 3(a) shows that the products are uniform and well-dispersive nanowires. The enlarged images (Fig. 3(b) and (c)) show that these nanowires have smooth surface and possess an average diameter of 100 nm and a length of several tens of micrometers. The EDX spectrum in Fig. 3(d) displays only strong Sb and Se peaks. The quantity analysis reveals that the atomic ratio of Sb:Se is quite close to 2:3, as expected. TEM image in Fig. 3(e) indicates the nanowire-like morphology of Sb_2Se_3, which agrees well with SEM results. High-resolution TEM image (Fig. 3(f)) indicates the single crystalline nature of Sb_2Se_3 nanowires. Meanwhile Sb_2Se_3 nanowires are confirmed to be single crystals with the [001] growth direction. The corresponding selected area electron diffraction (SAED, inset of Fig. 3(f)) taken from this nanowire can be indexed as an orthorhombic Sb_2Se_3 single-crystal recorded from the [−111] zone axis. The superb crystal quality of Sb_2Se_3 nanowires is highly anticipated to lead to improved lithium storage performance.

To investigate the formation mechanism of different interesting structures, we considered and studied the induced effects in each independent step, and interpreted the formation mechanism. As shown in Fig. 4, the synthesis of Sb_2Se_3 nanowires or Se microrods under microwave irradiation can be separated into three independent steps: (I) the mixture of antimony and selenium salts in EG/H_2O solvent; (II) the introduction of reducing agent $NaBH_4$ along with the nucleation of $(Sb_2Se_3)_n$; (III) subject to microwave irradiation. During Step I, Sb^{3+} would hydrolyze in aqueous solution and form into stable antimony complex, which is determinable for the exactly stoichiometric Sb_2Se_3. If subjected to the higher ratio of EG, as exemplified in sample E15 and E20 (Fig. 1(h) and (g)), trace amount of antimony element can be detected in the resulted products. It is supposed that most of Sb-salts would be removed during centrifugation and sample washing process. During Step II, the reducing agent $NaBH_4$ plays decisive roles through governing initial nucleation. It has been studied after $NaBH_4$ dissolves in solution, once BH_4^- is consumed and functions its ability to reduce metal salts into colloids, the pH values of solution tend to increase [34]. The pH value measurements demonstrated that the mixtures containing Sb-salts and Se-salts in EG-H_2O were all acid solutions (Table S2). After the introduction of $NaBH_4$, the pH value of E0, E5 and E10 mixture solutions was measured to be 10.2, 9.3 and 8.4 (i.e., all basic solutions). Whereas E15 and E20 mixture solutions were found to still remain acid suspensions with pH value of 5.7 and 4.8, respectively. The pH value changes suggest that in EG-excess mixture solution, such as E15 and E20 system, $NaBH_4$ is unable to completely function its reducing ability [35]. Therefore in this way, only Se colloids could be obtained instead of Sb_2Se_3.

Moreover, we collected intermediate products synthesized from the precursor solution with 3 h constant stirring at room temperature before microwave irradiation. As indicated in Fig. S2(a), S2(b) and S2(c), the diffraction peaks exhibit broad full width at half maximum (FWHM) and weak intensity, implying the amorphous state of products. It is conceivable that crystalline Sb_2Se_3 is difficult to be achieved at room temperature. However interestingly, XRD patterns of intermediate products synthesized from solution containing higher ratio EG display some diffraction peaks (Fig. S2(d) and Fig. S2(e)), suggesting that Se colloids were formed during this process even without microwave heating. SEM images demonstrated intermediate products synthesized from E0, E5 and E10 solution systems contained a lot of nanoparticles (Fig. S3(a), S3(b) and S3(c), respectively). Additionally, the product came from E15 solution system consisted of larger size irregular particles (Fig. S3d). Notably, intermediate product collected from pure EG system exhibit 1D rod structure (Fig. S3(e)), and corresponding point elemental analysis confirmed that the achieved products are almost Se (Fig. S3(g)), which is in agreement with previous XRD result. These results indicate that even at room temperature without microwave irradiation, hexagonal phase Se rods have already formed in EG-excess systems. Consequently it can be anticipated that excess amount of EG in the mixture solution prohibit $NaBH_4$ com-

Please cite this article as: W. Luo et al., Fast, green microwave-assisted synthesis of single crystalline Sb_2Se_3 nanowires towards promising lithium storage, Journal of Energy Chemistry (2018), https://doi.org/10.1016/j.jechem.2018.03.013

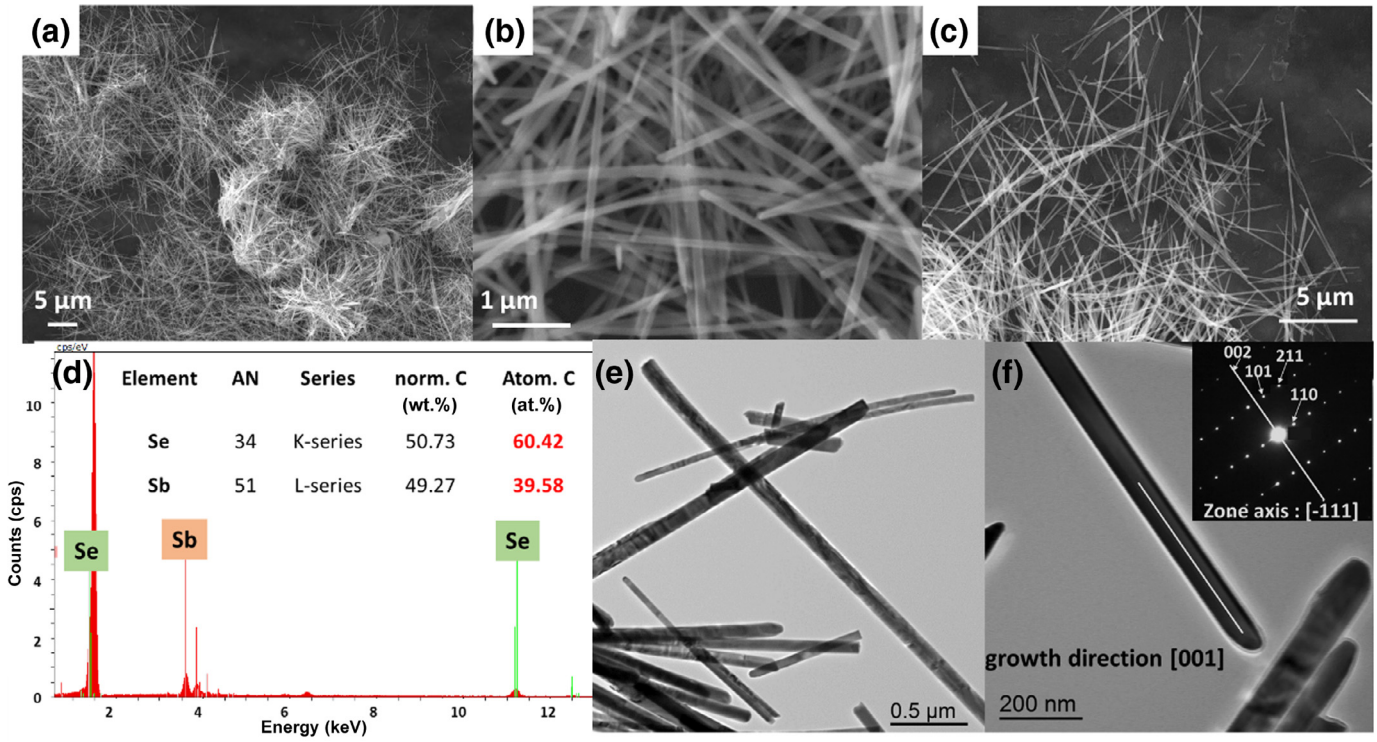

Fig. 3. SEM images (a)–(c), EDX spectrum and quantity analysis (d), TEM images (e, f) and select area electron diffraction (SAED) result (inset of Fig. 3(f)) of Sb_2Se_3 nanowires.

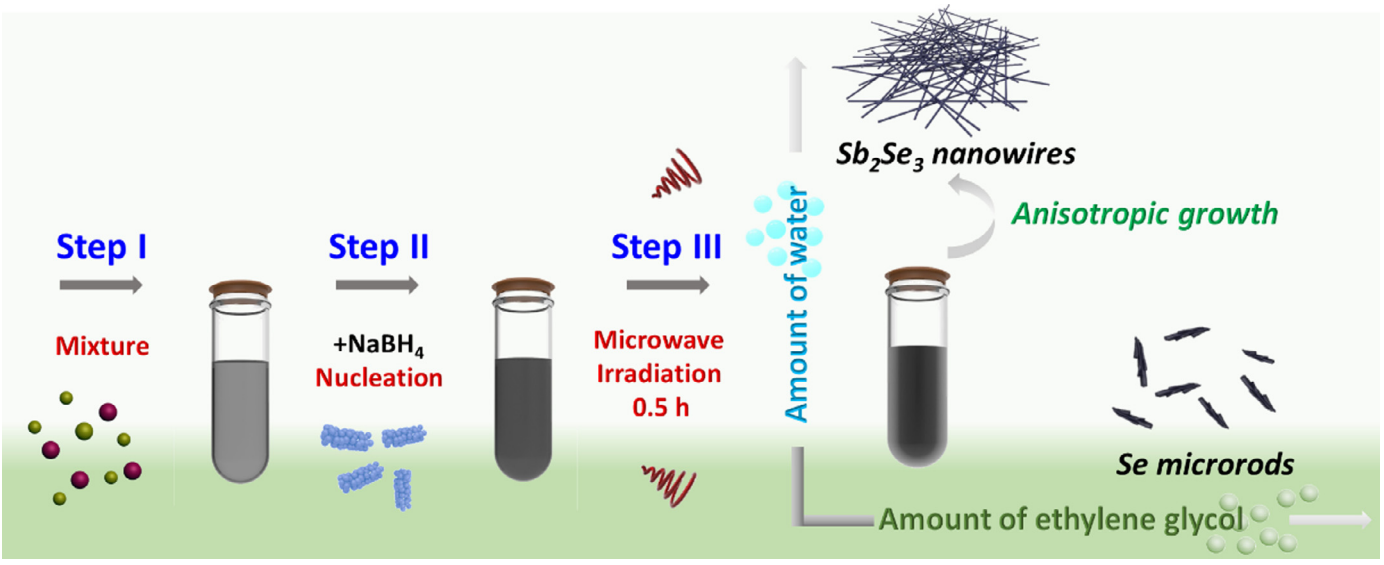

Fig. 4. Schematic illustration of synthesis procedure and formation mechanism of Sb_2Se_3 nanowire via solvent-mediated microwave irradiation.

pletely reduce SeO_3^{2-} into Se colloid neither contribute to form $(Sb_xSe_y)_n$ high-active colloids.

Lastly during a highly efficient microwave heating (Step III), water exhibits excellent microwave absorbance which would increase in the pressure, as it can be seen that an increase of ratio of H_2O in the reaction system would lead to the increase of pressure (Fig. S4). When the solutions containing amorphous nanoparticles were irradiated by microwave, the heat could be easily transferred from the water to the $(Sb_2Se_3)_n$ amorphous nanoparticles due to its excellent heat conductivity [36], which could also induce a rapid temperature increase on the surfaces and contribute to the anisotropic growth of Sb_2Se_3 nanowires.

Since Sb_2Se_3 has been demonstrated to be a promising high-capacity anode for LIBs, the high quality of achieved single crystalline nanowires inspires the investigation of their electrochemical performance. To evaluate the lithium storage properties of Sb_2Se_3 nanowires, 2016-type coin cells were assembled using Li foil as the counter electrode. Fig. 5(a) displays cyclic voltammograms (CV) of Sb_2Se_3 nanowires during the first four cycles for LIBs. During the first cathodic scan, one sharp peak located at 1.38 V and a small peak around 1.25 V can be attributed to Li^+ intercalation into Sb_2Se_3 host and the conversion from Sb_2Se_3 to Sb particles, respectively; the peak observed at 0.77 V is resulted from the alloying process between Li^+ and Sb [7,11]. Upon the first anodic scan, three

Please cite this article as: W. Luo et al., Fast, green microwave-assisted synthesis of single crystalline Sb_2Se_3 nanowires towards promising lithium storage, Journal of Energy Chemistry (2018), https://doi.org/10.1016/j.jechem.2018.03.013

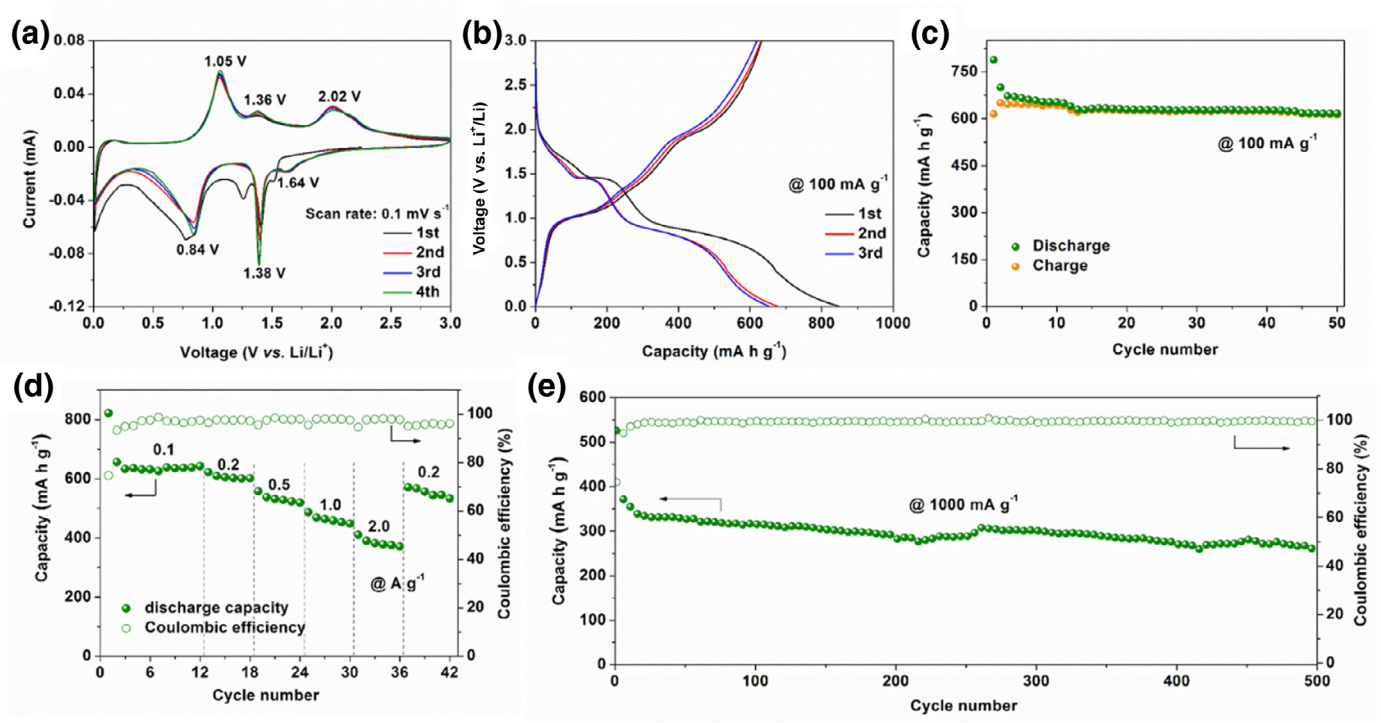

Fig. 5. Lithium storage performances of Sb_2Se_3 nanowires electrode: (a) Cyclic voltammogram curves at a scan rate of 0.1 mV s^{-1}; (b) first three charge–dischaege profiles at a current density of 100 mA g^{-1}; (c) cycling performance at a current density of 100 mA g^{-1}; (d) rate performances at various current densities; (e) long-term cycling performance at a current density of 1000 mA g^{-1}.

distinctive peaks located at 1.05, 1.36 and 2.02 V can be observed; specifically, the peak centred at 1.05 V corresponds to the dealloying process from Li_3Sb to Sb, while the peak located at 1.36 V relates to the conversion reaction between Li_2Se and Sb along with the formation of Li_x Sb_2Se_3, and the peak at 2.02 V is attributed to the Li^+ extraction and the final formation of Sb_2Se_3. In the following three cathodic scans, three reduction peaks at 1.64, 1.38 and 0.84 V can be detected, and the voltage difference between the first cycle and the following cycles due to the formation of solid electrolyte interphase (SEI) film [37]. From the second scan onward, the reduction and oxidation peaks are almost unchanged, suggesting a highly reversible nature of alloying and conversion reactions during the charge/discharge and thus the outstanding reversibility of Sb_2Se_3 nanowires electrode.

Fig. 5(b) shows the typical charge–discharge voltage profiles of Sb_2Se_3 nanowires for the first three cycles at a current density of 100 mA g^{-1}. The electrode provides a discharge and charge capacity of 846.5 and 632.2 mAh g^{-1}, respectively, corresponding to an initial Coulombic efficiency (CE) of 74.7%. Besides, the discharge profiles are characterized by a inclined plateau around 1.65 V (Li^+ intercalation) and two flat plateaus at 1.40 V (conversion reaction) and 0.84 V (alloying reaction), which are well in accordance with the above CV results. Fig. 5(c) demonstrates the cycling performance of Sb_2Se_3 nanowires at a current density of 100 mA g^{-1}. Sb_2Se_3 electrode delivers a reversible capacity of 672 mAh g^{-1} (based on 3rd reversible capacity) at 100 mA g^{-1}, which is quite close to its theoretical capacity of 670 mAh g^{-1}. Notably, Sb_2Se_3 nanowire electrode is capable to display a capacity retention of 91.8% after 50 cycles, revealing its good stability and high reversibility.

The rate performance is then evaluated by charging/discharging at various current densities, as demonstrated in Fig. 5(d). The average reversible capacities of Sb_2Se_3 electrode are 638.2, 611.5, 543.6 and 472.3 mAh g^{-1}, at current densities of 0.1, 0.2, 0.5 and 1.0 A g^{-1}, respectively. Impressively, even a high capacity of 389.5 mAh g^{-1} can be still achieved when a current density of 2.0 A g^{-1} is applied. The rate capability is even competitive to the reported Sb_2Se_3 anode [7] including some carbonaceous material or doping modified Sb_2Se_3 electrodes [38–40]. Additionally, the discharge capacity can be recovered to 574.1 mAh g^{-1} when the current density comes back at 0.1 A g^{-1}, which indicates a good reversibility of as-prepared Sb_2Se_3 electrode. Fig. 5(e) shows the long-term cyclability of Sb_2Se_3 nanowires at a relative high current density of 1000 mA g^{-1}. Notably, the Sb_2Se_3 electrode exhibits remarkable ultra-long cycling stability. It is to be pointed out that the as-fabricated Sb_2Se_3 nanowire electrode is lack of any carbon buffer layer modification, thus it is reasonable to observe the slight capacity fade during long-term cycle which is due to the surface reconstruction of Sb_2Se_3 nanowire and SEI film. The CE gradually increases during initial several cycles and then stabilizes around 99% in the upcoming long-term cycles. After 1000 cycles, the Sb_2Se_3 electrode can still deliver a reversible capacity of 260.8 mAh g^{-1}. The above electrochemical tests reveal that the as-synthesized high-quality single-crystalline Sb_2Se_3 nanowires exhibit great promise towards lithium storage.

In order to disclose the intrinsic mechanism of good cycling performance of Sb_2Se_3 nanowire electrode, EIS measurement was carried out. As shown in Fig. 6, the EIS plot of Sb_2Se_3 nanowire electrode is composed with an inclined line at low frequency and two depressed semicircles at high frequency region. The inclined line is associated to the diffusion of Li ions in the bulk of the electrode material, and the diffusion coefficient value (D) of the Li ions can be calculated based on the equation: $D = 0.5(RT/An^2F^2\sigma_W C)^2$, where R is the gas constant, T is the temperature, A stands for the area of the electrode surface, n is the number of electrons transferred per mole of the active material involved in the electrochemical reaction, F is the Faradic constant, σ_W is the Warburg coefficient, and C is the molar concentration of Li ions [41,42]. The apparent Li ion diffusion coefficient for Sb_2Se_3 nanowires electrode is calculated to be 1.03×10^{-10} cm^2 s^{-1}, suggesting the fast and effi-

Please cite this article as: W. Luo et al., Fast, green microwave-assisted synthesis of single crystalline Sb_2Se_3 nanowires towards promising lithium storage, Journal of Energy Chemistry (2018), https://doi.org/10.1016/j.jechem.2018.03.013

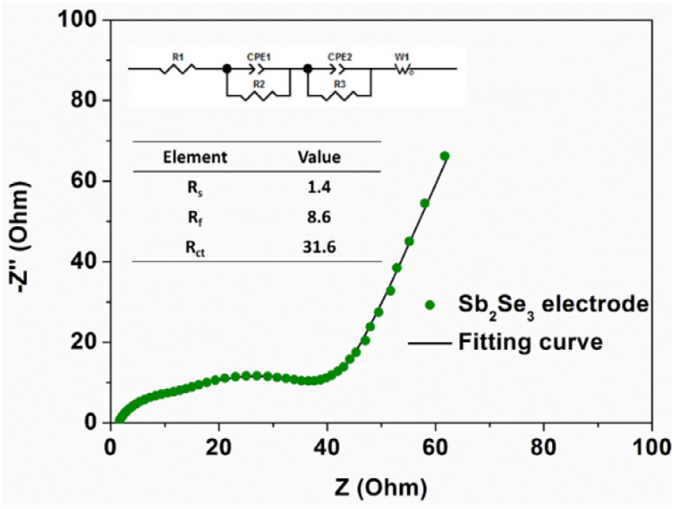

Fig. 6. EIS plot and the corresponding fitting curve of Sb_2Se_3 electrode (inset are the equivalent circuit and a summary of simulation results of resistance value).

cient lithium diffusion process within the electrode. The first one semicircle observed in the medium-to-high frequency corresponds to the interfacial resistance between the electrode and electrolyte (R_f). The second semicircle appearing in the low frequency is due to the charge transfer resistance (R_{ct}). And the bulk resistance (R_s) of Li-Sb_2Se_3 battery is the intercept at the real axis [43,44]. After simulation, the values of R_s, R_f and R_{ct} were determined to be 1.4, 8.6 and 31.6 Ω, which confirm the excellent electrical conductivity and the good interfacial contact of SEI film formed in the cell of Li–Sb_2Se_3, thus resulting in its long-term cycling stability and good rate performance.

4. Conclusions

In summary, this work offers a rapid, green, inexpensive and highly reproducible approach for the synthesis of uniform single crystalline Sb_2Se_3 nanowires. The achieved uniform Sb_2Se_3 nanowires are single crystalline along [001] growth direction with a diameter of 100 nm and a length up to tens of micrometers. Through merely varying the volume ratio of solvents in a simple EG/H_2O solvent system, Sb_2Se_3 nanowires and Se microrods can be easily achieved. Significantly, when evaluated as an anode of LIBs, Sb_2Se_3 nanowires can deliver a high reversible capacity of 650.2 mAh g^{-1} at 100 mA g^{-1} and a capacity retention of 63.8% after long-term 1000 cycles at 1000 mA g^{-1}, as well as superior rate capability (389.5 mAh g^{-1} at 2000 mA g^{-1}), which show great potential as a promising candidate for high-performance LIBs. At last we believe our facile strategy can be easily extended towards the preparation of other nanoscale advanced nanomaterials for energy storage and conversion.

Acknowledgments

This work was supported by the National Key Research and Development Program of China (2016YFA0202603), the National Basic Research Program of China (2013CB934103), the National Natural Science Foundation of China (51521001, 51602239), the National Natural Science Fund for Distinguished Young Scholars (51425204), Yellow Crane Talent (Science & Technology) Program of Wuhan City and the Fundamental Research Funds for the Central Universities (WUT: 2016III001, 2016III003, 2016IVA090) and the Programme of Introducing Talents of Discipline to Universities (B17034). We acknowledge the funding support from the Lorraine Region (now part of Grand Est Region) Cooperation Research Lorraine/Hubei Program 2015/2017.

Declarations of interest

None

Supplementary materials

Supplementary material associated with this article can be found, in the online version, at doi:10.1016/j.jechem.2018.03.013.

References

[1] K. Mitchell, J.A. Ibers, Chem. Rev. 102 (2002) 1929–1952.
[2] T. Zhai, M. Ye, L. Li, X. Fang, M. Liao, Y. Li, Y. Koide, Y. Bando, D. Golberg, Adv. Mater. 22 (2010) 4530–4533.
[3] T.Y. Ko, M. Shellaiah, K.W. Sun, Sci. Rep. 6 (2016) 35086.
[4] Y. Zhou, L. Wang, S. Chen, S. Qin, X. Liu, J. Chen, D.J. Xue, M. Luo, Y. Cao, Y. Cheng, Nat. Photonics 9 (2015) 409–415.
[5] Y.C. Choi, T.N. Mandal, W.S. Yang, Y.H. Lee, S.H. Im, J.H. Noh, S.I. Seok, Angew. Chem. In. Ed. 53 (2014) 1329–1333.
[6] M.R. Gao, Y.F. Xu, J. Jiang, S.H. Yu, Chem. Soc. Rev. 42 (2013) 2986–3017.
[7] W. Luo, A. Calas, C. Tang, F. Li, L. Zhou, L. Mai, ACS Appl. Mater. Interfaces 8 (2016) 35219–35226.
[8] J. Ma, Y. Wang, Y. Wang, Q. Chen, J. Lian, W. Zheng, J. Phys. Chem. C 113 (2009) 13588–13592.
[9] G. Chen, J. Zhou, J. Zuo, Q. Yang, ACS Appl. Mater. Interfaces 8 (2016) 2819–2825.
[10] Z. Chen, F. Chen, N.D. Tan, J. Mater. Sci. Mater. Electron. 26 (2015) 970–977.
[11] X. Ou, C. Yang, X. Xiong, F. Zheng, Q. Pan, C. Jin, M. Liu, K. Huang, Adv. Funct. Mater. 27 (2017) 1606242.
[12] H.W. Chang, B. Sarkar, C. Liu, Cryst. Growth Des. 7 (2007) 2691–2695.
[13] D. Wang, D. Yu, M. Shao, W. Yu, Y. Qian, Chem. Lett. 31 (2002) 1056–1057.
[14] M. Chen, L. Gao, Mater. Res. Bull. 40 (2005) 1120–1125.
[15] Y. Yu, R. Wang, Q. Chen, L.M. Peng, J. Phys. Chem. B 110 (2006) 13415–13419.
[16] Q. Xie, Z. Liu, M. Shao, L. Kong, W. Yu, Y. Qian, J. Crys. Growth 252 (2003) 570–574.
[17] J. Ma, Y. Wang, Y. Wang, P. Peng, J. Lian, X. Duan, Z. Liu, X. Liu, Q. Chen, T. Kim, CrystEngComm 13 (2011) 2369–2374.
[18] Y. Liang, Y. Wang, J. Wang, S. Wu, D. Jiang, J. Lian, RSC Adv. 6 (2016) 11501–11506.
[19] L. Qi, Coordin. Chem. Rev. 254 (2010) 1054–1071.
[20] C. Zhao, X. Cao, X. Lan, Mater. Lett. 61 (2007) 5083–5086.
[21] Y.Q. Liu, M. Zhang, F.X. Wang, G.B. Pan, J. Mater. Chem. C 2 (2014) 240–244.
[22] P. Kulal, D. Dubal, V. Fulari, J. Mater. Sci. 46 (2011) 2789–2795.
[23] W. Farfán, E. Mosquera, R. Vadapoo, S. Krishnan, C. Marín, J. Nanosci. Nanotechnol. 10 (2010) 5847–5850.
[24] X. Wang, K. Cai, H. Liu, Crys. Growth. Des. 11 (2011) 4759–4767.
[25] S.A. Galema, Chem. Soc. Rev. 26 (1997) 233–238.
[26] Z. Ni, R.I. Masel, J. Am. Chem. Soc. 128 (2006) 12394–12395.
[27] M. Baghbanzadeh, L. Carbone, P.D. Cozzoli, C.O. Kappe, Angew. Chem. In. Ed. 50 (2011) 11312–11359.
[28] G.A. Tompsett, W.C. Conner, K.S. Yngvesson, ChemPhysChem 7 (2006) 296–319.
[29] B. Zhou, J.J. Zhu, Nanotechnology 20 (2009) 085604.
[30] C.P. Yang, S. Xin, Y.X. Yin, H. Ye, J. Zhang, Y.G. Guo, Angew. Chem. In. Ed. 52 (2013) 8363–8367.
[31] J. Qian, K.J. Jiang, J.H. Huang, Q.S. Liu, L.M. Yang, Y. Song, Angew. Chem. In. Ed. 51 (2012) 10351–10354.
[32] I. Efthimiopoulos, J. Zhang, M. Kucway, C. Park, R.C. Ewing, Y. Wang, Sci. Rep. 3 (2013) 2665.
[33] G. Lucovsky, A. Mooradian, W. Taylor, G. Wright, R. Keezer, Solid State Commun. 5 (1967) 113–117.
[34] H.J. Shin, K.K. Kim, A. Benayad, S.M. Yoon, H.K. Park, I.S. Jung, M.H. Jin, H.K. Jeong, J.M. Kim, J.Y. Choi, Adv. Funct. Mater. 19 (2009) 1987–1992.
[35] Y. Jiang, W. Zeng, Y. Fang, Chem. Lett. 43 (2013) 111–112.
[36] S. Xiao, P. Liu, W. Zhu, G. Li, D. Zhang, H. Li, Nano Lett. 15 (2015) 4853–4858.
[37] W. Luo, P. Zhang, X. Wang, Q. Li, Y. Dong, J. Hua, L. Zhou, L. Mai, J. Power Sources 304 (2016) 340–345.
[38] R. Jin, Z. Liu, L. Yang, J. Liu, Y. Xu, G. Li, J. Alloys Compd. 579 (2013) 209–217.
[39] M. Xue, Z. Fu, J. Alloys Compd. 458 (2008) 351–356.
[40] Y. Le, C. Jie, Z. Fu, Electrochim. Acta 55 (2010) 1258–1264.
[41] X. Ou, X. Liang, F. Zheng, Q. Pan, J. Zhou, X. Xiong, C. Yang, R. Hu, M. Liu, Chem. Eng. J. 320 (2017) 485–493.
[42] C. Yang, X. Ou, X. Xiong, F. Zheng, R. Hu, Y. Chen, M. Liu, K. Huang, Energy Environ. Sci. 10 (2017) 107–113.
[43] Y. Bai, X. Wang, X. Zhang, H. Shu, X. Yang, B. Hu, Q. Wei, H. Wu, Y. Song, Electrochim. Acta 109 (2013) 355–364.
[44] T. Liu, A. Garsuch, F. Chesneau, B.L. Lucht, J. Power Sources 269 (2014) 920–926.